

## GRAPHICAL ABSTRACT

### Comparative docking of SARS-CoV-2 receptors antagonists from repurposing drugs

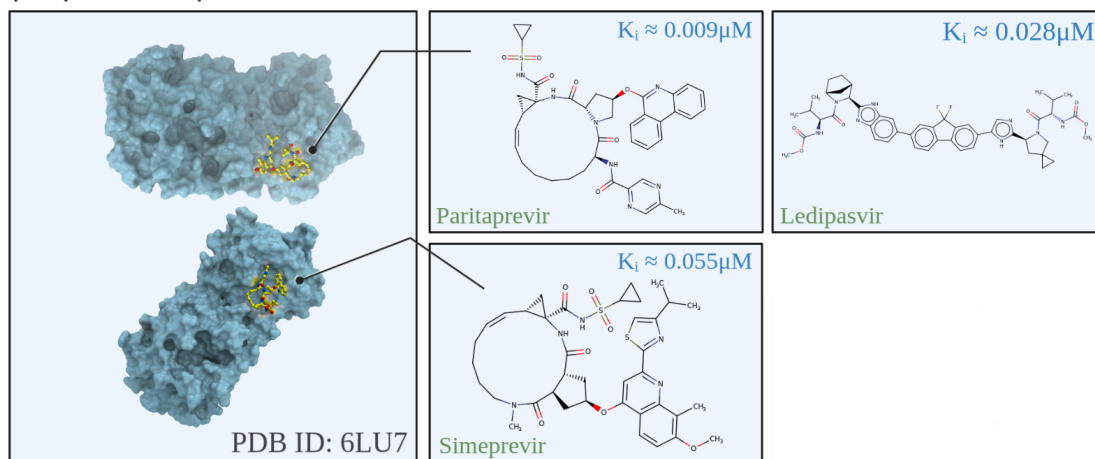
Micael D. L. Oliveira <sup>a</sup> and Kelson M. T. Oliveira <sup>a</sup>

<sup>a</sup> Laboratory of Theoretical and Computational Chemistry. Department of Chemistry, Federal University of Amazonas, 69077-000, Manaus, AM, Brazil;

#### ARTICLE HISTORY

Compiled May 3, 2021

SARS-CoV-2 Mpro in complex with paritaprevir and simeprevir



## RESEARCH ARTICLE

# Comparative docking of SARS-CoV-2 receptors antagonists from repurposing drugs

Micael D. L. Oliveira <sup>a</sup> and Kelson M. T. Oliveira <sup>a</sup>

<sup>a</sup> Laboratory of Theoretical and Computational Chemistry. Department of Chemistry, Federal University of Amazonas, 69077-000, Manaus, AM, Brazil

### ARTICLE HISTORY

Compiled May 3, 2021

### ABSTRACT

SARS-CoV-2 is the seventh coronavirus to infect humans. Currently, there are no pharmacological treatments proven against COVID-19 or that may be of a broad spectrum to minimize the sequelae. This work aims to identify compounds or drugs already commercialized that may be supporting in the treatment of infectious conditions of COVID-19, parallel to the administration of vaccines. In this context, molecular docking simulations were carried out to understand which drugs are most effective in modulating a total of ten receptors, whether directly in viral, pro-inflammatory or central nervous system signaling, related to COVID-19. Subsequently, some results were validated through molecular dynamics simulations based on publicly available trajectory files. Among a total of 71 molecular docking simulations, the drug ledipasvir administered to patients with Hepatitis-C (HCV) was the most promising with a mean value  $\Delta G^\circ \approx -10.3 \text{ kcal} \cdot \text{mol}^{-1}$  and a nonspecific probability according to neural networks of 0.21. Ivermectin, although it had an average affinity of  $-9.6 \text{ kcal} \cdot \text{mol}^{-1}$ , was shown to be a ligand with a very expressive degree of nonspecificity of 0.93. When analyzing the atomic fluctuations of molecular dynamics, telaprevir stood out for the large number of rotational freedom in line with expressive RMSF fluctuations with a peak around  $20 \text{ \AA}$  in the interaction with the Spike protein. Consequently, it was shown to be superior to the various anecdotally reported medications, such as nitazoxanide, and that due to the low mobility, the affinity was not so expressive due to the relative high fluctuations of  $10 \text{ \AA}$ . Fi-

nally, these results seek to clarify from a theoretical point of view the interaction of numerous medications from viral signaling to the neuroinflammatory system.

## **KEYWORDS**

SARS-CoV-2; Neuroinflammation; Molecular docking; Molecular dynamics; Ledipasvir.

**Abbreviations:** ACE2, Angiotensin-converting enzyme 2; RdRp, RNA-dependent RNA polymerase; Mpro, Main protease; 3CLpro, 3-chymotrypsin-like protease;

## **1. Observations**

Observations: This work is not conclusive and is only computational simulations. Under no circumstances should we extrapolate *in silico* studies into clinical practice, as it would violate medical ethics principles. The main conclusion was that some drugs can be classified as false positives as predicted on the Hit Dexter 2.0 platform. Our main example is ivermectin, where the probability of nonspecificity is extremely high, thus leading to hasty and erroneous conclusions.

## **2. Introduction**

The first cases of hospitalization for SARS-CoV-2 infections were reported in December 2019 in Wuhan, Hubei province, China. This virus is of a proportion not seen since the Spanish Flu pandemic in 1918 (Li et al., 2020). The coronavirus (CoV) belongs to the family Coronaviridae, of the order Nidovirales, which are single-stranded RNA viruses (Zhu et al., 2020). The onset of severe acute respiratory syndrome (SARS) occurred about 18 years ago, and the genetic sequences are very similar to the virus that causes COVID-19, sharing about 79.6% homology with SARS-CoV-1 (Zhou et al., 2020). Infection with COVID-19 causes severe and systemic respiratory failure and is associated with high mortality. The infection has a more likely replication in elderly patients with comorbidities (Chen, Liu, & Guo, 2020).

Patients with COVID-19 commonly present neurological manifestations, such as dizziness, headache, impaired consciousness and seizure. In addition, those with the most severe form of the infection had a more pronounced inflammatory response, in-

cluding lower lymphocyte counts and significantly higher pro-inflammatory cytokines compared to patients with milder infection. This phenomenon may be indicative of immunosuppression in these patients (Mao et al., 2020). Encephalopathy has been reported, as well as Guillain-Barré syndrome and acute cerebrovascular disease, have also emerged as a serious complication. It was noticed that often strokes in patients are due to an elevated pro-inflammatory state (Ellul et al., 2020). In addition, the coronavirus is able to spread in the olfactory epithelium towards the central nervous system (Zubair et al., 2020). After preliminary analyzes of the immunological patterns of patients with the most severe symptoms of COVID-19, the researchers realized that pro-inflammatory proteins present in the system, were expressed in higher concentrations, in particular, interleukin 6 (Xu et al., 2020). Recent research has found that with advanced age, the expression of the ACE2 protein increases, as well as the TMPRSS2 gene in animal models (Bilinska, Jakubowska, Bartheld, & Butowt, 2020). Concomitantly, a group of researchers found that the neuropilin-1 cell receptor (NRP1) can significantly increase the virulence of SARS-CoV-2. The study in mice demonstrated the transport of viral particles, mediated by NRP1, towards the central nervous system (Cantuti-Castelvetri et al., 2020).

Since COVID-19 can attack various systems, in this study we evaluated, using the molecular docking tool, a set of medications interacting with receptors present in viral signaling, but also pro-inflammatory and the central nervous system. Furthermore, it was calculated the prediction of the degree of specificity of interaction and subsequent analysis of the chemical interactions that were formed in the receptor-ligand complex. Finally, through molecular dynamics simulations, it was possible to validate the results obtained by docking. It is worth clarifying that the molecular docking technique is a theoretical methodology that allows investigating, by means of computational models, which active site of a protein or enzyme is more likely to be occupied by a given compound or ligand. The first docking algorithms were developed throughout 1980, having been essential in the discovery of captopril, the first computationally constructed medication (Patrick, 2013). The main question of all docking programs is to address which combination of orientation and conformation is the most favorable in relation to all other possible combinations (conformers) (Perola, Walters, & Charifson, 2004). In this

way, the molecular docking algorithms perform a search algorithm in which the conformation of the ligand is evaluated recursively until the convergence to the minimum energy is reached. Finally, is employed an affinity scoring function, where the state variable  $\Delta G^\circ(kcal \cdot mol^{-1})$  is used to classify the most favorable orientations, so that more negative values denote greater spontaneity and favoring molecular interaction (Pagadala, Syed, & Tuszynski, 2017).

Fully considering the flexibility of the receptor still represents one of the great limitations of molecular docking. Although we have adopted docking with degrees of rotational freedom to the ligands, molecular dynamics simulations are still essential to validate the docking results. In this context, throughout the research, we also used molecular dynamics to investigate the structural stability of the complex as a function of time (Serdyuk, Zaccai, & Zaccai, 2007). Molecular dynamics has been a well-known and reliable methodology since 1975 when M. Karplus and his research group carried out the first molecular dynamics simulation in the biomolecular context, but limited to computational resources at the time (McCammon, Gelin, & Karplus, 1977). In molecular dynamics, successive iterations are generated by the integration of Newtonian laws of motion consisting of 4 (four) central steps:

- I. minimization: releasing excess tension from the system;
- II. heating: raising the system temperature to a specific condition;
- III. equilibration: balances the system before energy properties can be measured;
- IV. production: final stage that simulates the dynamics of the studied system (Leach, 2001).

### **3. Materials and methods**

#### ***3.1. Protocols of molecular docking***

All the crystallographic structures used in this research were obtained from the Protein Data Bank (PDB) database (Berman et al., 2000) and whose visualization can be found in (see Figure 1). As a result of the absence of crystallographic structures for the TMPRSS2 protein, we performed a computational prediction. Initially, the amino

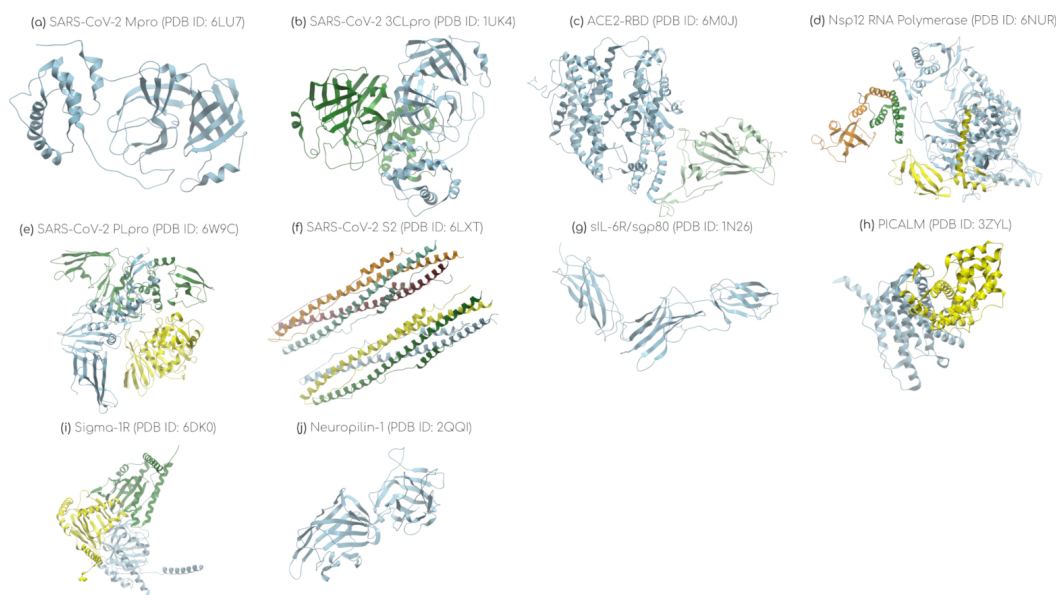


**Figure 1.** Visualization of the crystallographic structures solved by experimental methods by researchers all over the world, which were essential in all computer simulations in this research. The structural visualization was possible with the free version of the Molsoft ICM-Browser software.

acid sequence was obtained from the UniProt database (<https://www.uniprot.org/>) in FASTA format, with the code TMPS2\_HUMAN. Through the Robetta server (<http://rosetta.bakerlab.org/>) it was possible to predict the crystallographic structure of the enzyme. Due to the lack of structures with a high degree of homology, the ab-initio modeling method of the RosettaCM algorithm (Song et al., 2013) was chosen. The structural validation of the conformational prediction (see Figure 2) was performed using the RAMPAGE platform (Ramachandran Plot Investigation) (Lovell et al., 2003). Among a total of 490 residues that constitute the TMPS2 protease, a group of 403 residues (82.2%) was present in a region without steric impediments. It is noted that a number above (98%) is recommended in the most favorable region (Lovell et al., 2003). Therefore, although the conformational prediction has some limitations, we can consider it to be consistent for the simulations.

The latest version of AutoDock Vina 1.1.2 was adopted (Trott & Olson, 2010) in the docking methodology, being an efficient and widely used docking tool. The PubChem database (Bolton et al., 2011) (<https://pubchem.ncbi.nlm.nih.gov/>) was important for obtaining the planar structure of all medications. The conformer was generated with an MMFF94 molecular mechanics method (Merck Molecular Force Field)

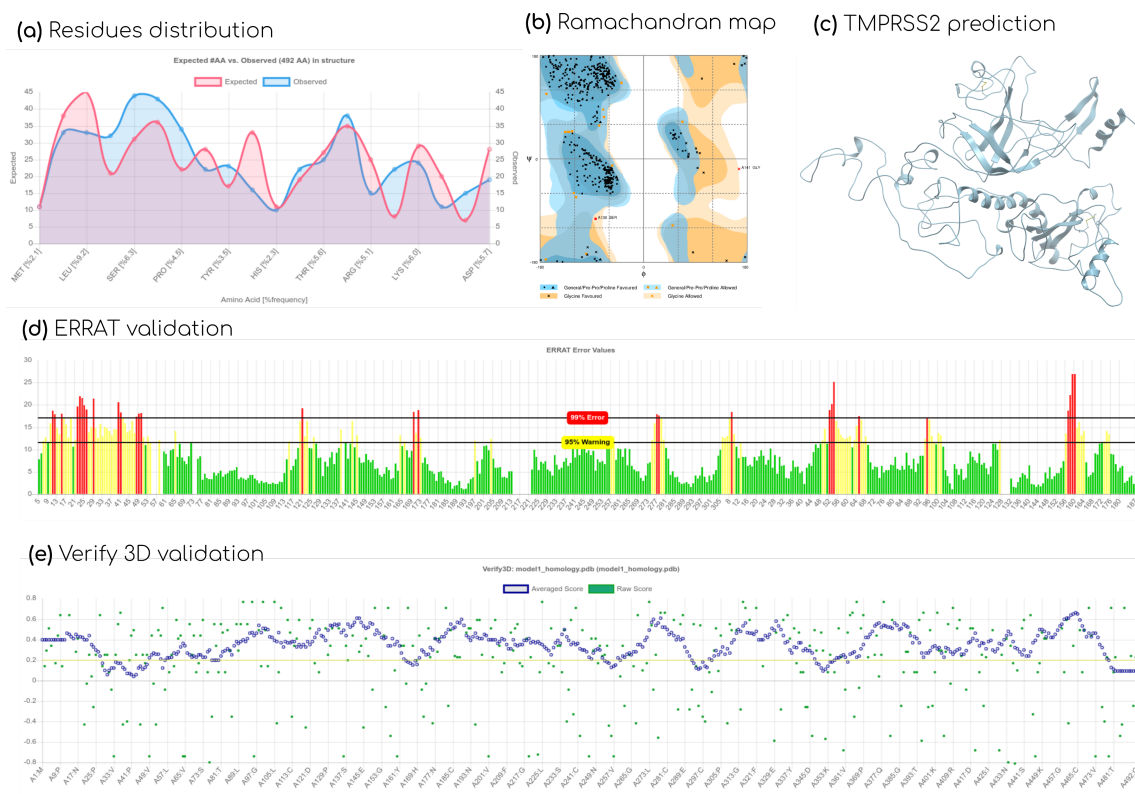


**Figure 2.** Structural validation of the TMPRSS2 protease regarding the prediction made by Rosetta CM and validated through SAVES v5.0 and RAMPAGE platform.

available in the MarvinSketch 20.10 software. The docking input files were prepared using the AutoDock Tools (ADT) 1.5.7-rc1 tool (Sanner, 1999). In this way, polar hydrogen atoms were added to the structure, while the nonpolar ones were removed. In addition, water molecules, cofactors and co-crystallized inhibitors were removed and partial charges of Gasteiger-Marsilli were attributed to the receptors and ligands. It is noted that all docking protocols follow as proposed by the developers themselves (Forli et al., 2016).

Although the side chains of the receptors were considered rigid, all degrees of rotational freedom were attributed to the ligands. The simulations were carried out in a single step, so that the docking was performed considering the coordinates of the grid box to the geometric center of the main binding site of each receptor, with a volume of  $(126.0\text{\AA})^3$  as a search space. In addition, we used an exhaustivity value of 400 and the pseudo-random seed was set to zero in all simulations to ensure reproducibility. Among the conformers resulting from docking, the one with the smallest  $\Delta G^\circ$  was chosen. In

order to validate the docking protocols, a re-docking of the co-crystallized ligands was performed for some proteins. All the predictions of the residues that constitute the receptor binding site were adopted using the fPocket algorithm through the Voronoi diagrams (Guilloux, Schmidtke, & Tuffery, 2009) (see Table 1).

All amino acid interactions were obtained using the ProteinPlus platform (<https://proteins.plus/>) (Stierand, Maaß, & Rarey, 2006) with the PoseView module. A more in-depth study of the amount of intermolecular interactions was possible with Arpeggio (<http://biosig.unimelb.edu.au/arpeggioweb/>) predicting interactions within a 5.0Å radial section (Jubb et al., 2017).

**Table 1.** Amino acids interacting with the most likely binding site at a cutoff distance of 2Å. The coordinates correspond to the centre of mass of each connection site. In addition, the ACE2-RBD complex (PDB ID: 6M0J) had its chains analyzed separately to predict the respective binding site of each protein.

Receptor	Cartesian coordinates
SARS-CoV-2 Mpro (PDB ID: 6LU7) (Liu et al., 2020)	$x = -47.232; y = -1.025; z = 47.896$
SARS-CoV-2 S (PDB ID: 6M0J) (X. Wang et al., 2020)	$x = -37.015; y = 42.687; z = 12.916$
ACE2 (PDB ID: 6M0J) (X. Wang et al., 2020)	$x = -14.764; y = 15.986; z = -3.539$
SARS-CoV-2 PLpro (PDB ID: 6W9C) (Osipiuk et al., 2020)	$x = -20.546; y = 10.027; z = 35.228$
SARS-CoV-2 S2 (PDB ID: 6LXT) (Xia et al., 2020)	$x = 10.747; y = -9.241; z = -23.509$
TMPRSS2	$x = 22.146; y = 3.117; z = 4.967$
sIL-6R (PDB ID: 1N26) (Varghese et al., 2002)	$x = 27.697; y = 47.105; z = 62.865$
PICALM (PDB ID: 3ZYL) (Miller, Sahlender, Graham, Robinson, & Peden, 2011)	$x = 12.479; y = -2.025; z = 42.479$
Sigma-1R (PDB ID: 6DK0) (Schmidt, Betz, Dror, & Kruse, 2018)	$x = -7.049; y = 33.830; z = -32.554$
Neuropilin-1 (PDB ID: 2QQI) (Appleton et al., 2007)	$x = -3.705; y = 20.874; z = 5.879$
NLRP3 (PDB ID: 3QF2) (Bae & Park, 2011)	$x = -11.123; y = 28.731; z = 42.849$

It is noted that we also perform docking under receptors not directly involved in viral signaling to attest to the specific interaction of medications. Thus, the structure adopted for the 5- $HT_{1B}$  serotonin receptor has PDB ID: 4IAQ with 2.8Å resolution obtained by X-ray diffraction and solved by (C. Wang et al., 2013). The search space was centered on the coordinates of the most likely link site ( $x = -9.528; y = 14.127; z = 6.899$ ), as predicted by the fPocket algorithm. We also chose the ionotropic glutamate 2 receptor with PDB ID: 5H8S with a resolution of 1.70Å solved by (Hackos et al., 2016) and whose site presented the coordinates in ( $x = 21.491; y = 6.032; z = 40.645$ ). All simulations were performed using the search space  $(126\text{Å})^3$  located from the binding site for each receptor.

### ***3.2. Protocols of molecular dynamics***

The trajectory files referring to MD protein-ligand simulations were made available by the D. E. Shaw Research group as open access (<https://www.deshawresearch.com/>) (D. E. Shaw Research, 2020). As described by the authors themselves, and regarding the files selected in this research, only the implicit solvation of the water molecules was considered, in addition to the presence of the metal cofactor Zinc while the receptor was the trimeric complex of the peak glycoprotein (S) in the closed conformation (PDB ID: 6VXX) described by the Amber ff99SB force field. The system was neutralized by the addition of  $Na^+$  and  $Cl^-$  ions at a physiological concentration of  $0.15\text{mol} \cdot L^{-1}$ . From the structure resulting in the equilibration of the protein-ligand complex, trajectories were calculated. Thus, the simulations were carried out at a temperature of 310K with the NPT ensemble in the range of approximately  $2\mu s$ . Throughout the RMS analyzes, they were all in relation to the  $C\alpha$  of the protein-ligand complex, where frame 0 was adopted as a reference. The estimated error in the RMSD, RMSF and Hydrogen bond values was based on the standard deviation of the measurements over time.

Through these important results we were able to study more deeply some of the medications present in molecular docking, and thus, validate the results. The analysis of trajectories and construction of graphs were possible with the libraries MDAnalysis (Michaud-Agrawal, Denning, Woolf, & Beckstein, 2011) and Matplotlib implemented in the Python 3 programming language. The number of Hydrogen bonds was estimated through a plugin in the VMD 1.9.4a.51 software where the donor-acceptor distance was  $3.0\text{\AA}$  while the cutoff angle was  $20^\circ$ .

## **4. Results and Discussions**

### ***4.1. Estimation of the relative value of $\Delta G^\circ$ using molecular docking***

First of all, we must highlight that the option to study other signaling pathways in molecular docking is a consequence of few computational studies on the signaling of the nervous or pro-inflammatory system related to COVID-19. Initially, there was a concern with the validation of the docking results, so it was important to carry out an

additional analysis via re-docking (see Figure 3). From the results, we concluded that the prediction of the conformer had an RMSD, in fact, lower than 2Å in relation to the co-crystallized ligand, being, therefore, in accordance with the value recommended in the literature (Bursulaya, Totrov, Abagyan, & Brooks, 2003). The minimization of errors in docking was due to the analysis of numerous receptors and the adoption of high exhaustiveness to reduce, as far as possible, the bias.

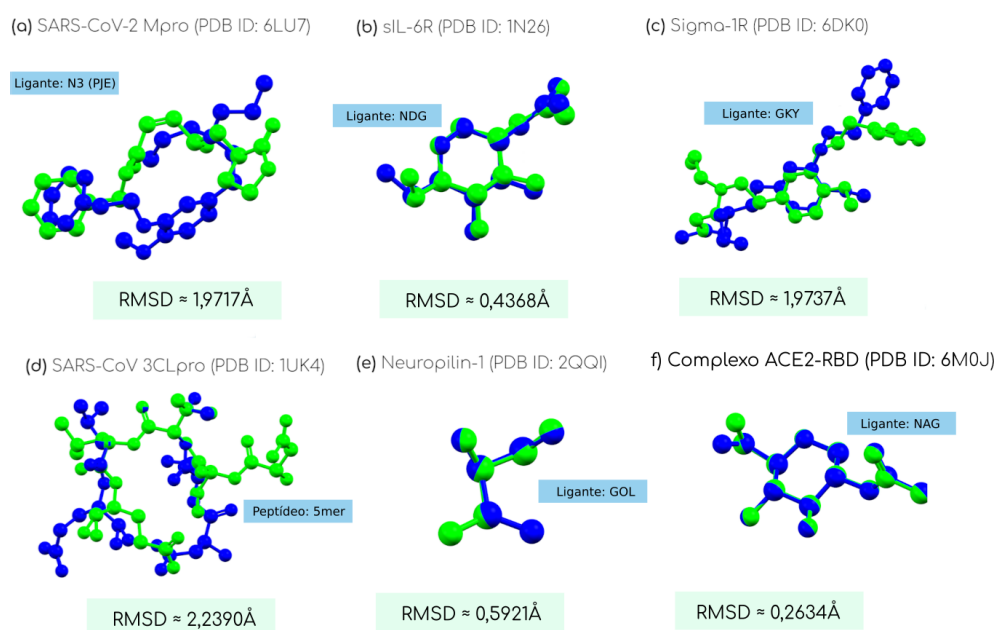


**Figure 3.** Results of the re-docking through the visualization of the structural alignment between the conformer (lowest  $\Delta G^\circ$ ) theoretically obtained via docking and the respective co-crystallized ligand. Using the LS-Align (Hu et al., 2018) platform, the value of *RMSD* was obtained. The graphical visualization took place through the academic version of the Mercury 4.3.0 software.

The docking results were organized so that the most negative mean values of  $\Delta G^\circ$  binding were allocated at the top (see Figure 4), indicating which compounds interact most spontaneously with the receptor. The best interaction with the viral receptors occurred with the antiviral ledipasvir, highlighted with the protease 3CLpro, TMPRSS2 and Neuropilin-1. Among 71 medications, only a total of 21 met our selection criteria ( $\Delta G^\circ \leq -9.0kcal \cdot mol^{-1}$ ) and thus indicating an expressive binding affinity against the studied enzymes.

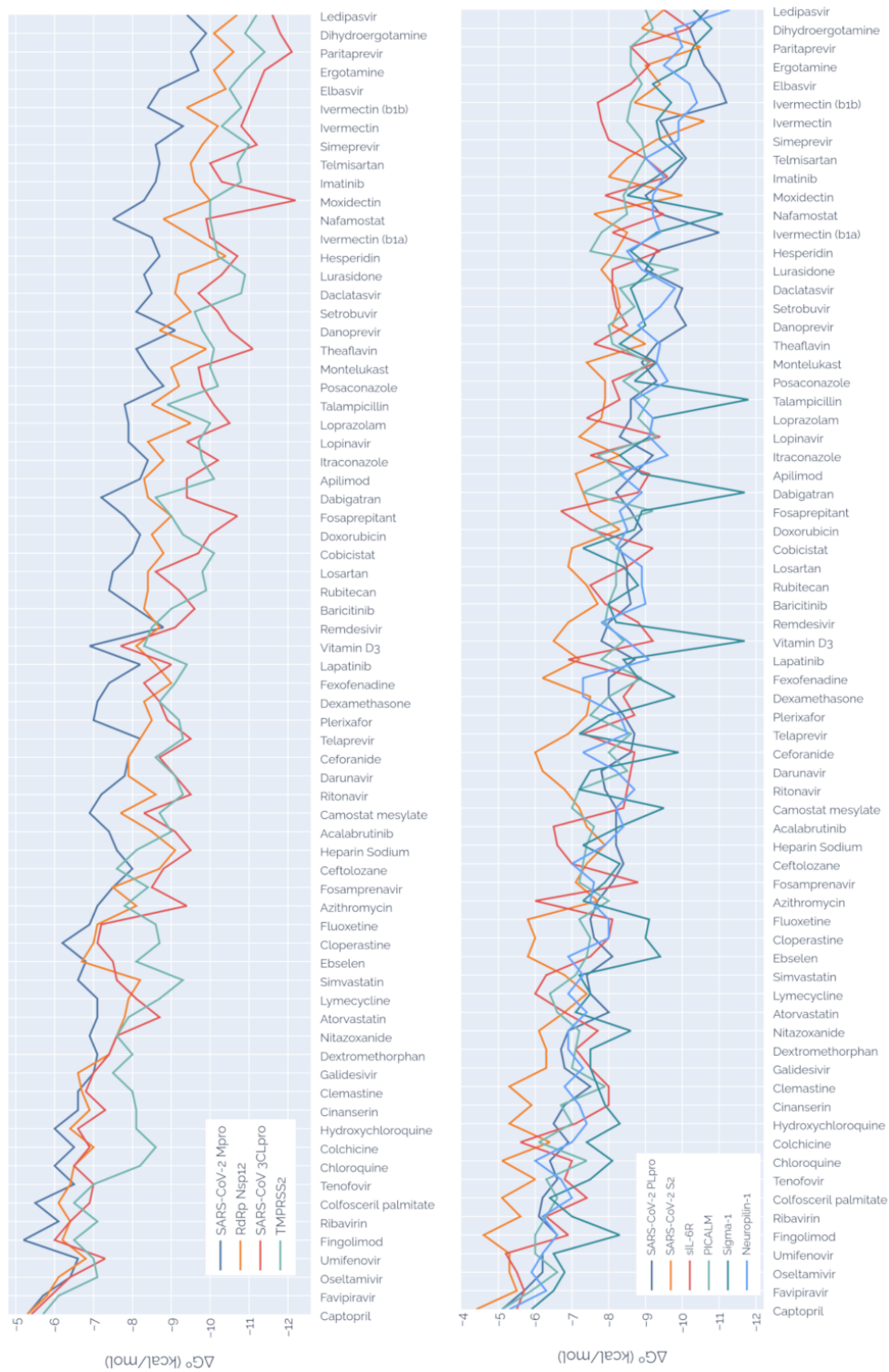


**Figure 4.** Line chart highlighting how the average value of  $\Delta G^\circ$  of the interaction varies between the ligand-receptor complexes studied. Note that the ligands have been ordered in ascending order of interaction affinity (from top to bottom). It should be noted that  $\Delta G^\circ$  values are relative and have a higher uncertainty associated with them, and therefore cannot be seen as absolute.

#### *4.1.1. The paradoxical results of ivermectin*

Among the most unexpected conclusions is ivermectin, which probably due to its large molecular geometry favors a greater probability of some polar contacts with different receptors, but it could also be inevitably more susceptible to adverse effects under high concentrations. Although the *in silico* results are very promising, pharmacokinetic factors limit the efficacy in clinical studies of ivermectin against COVID-19 (Schmith, Zhou, & Lohmer, 2020). Interestingly, ivermectin is reported to be effective against many single-stranded RNA viruses, such as Zika, Dengue, yellow fever, Chikungunya and even the human immunodeficiency virus (HIV) (Heidary & Gharebaghi, 2020). It is important to note that the decrease in ACE2 protein increases pathological susceptibility to arterial hypertension and myocardial infarction. Therefore, it is a possible adverse effect resulting from medications that interact remarkably with this receptor and when administered in high concentrations (W. Wang et al., 2012). The only drug that interferes with viral replication, without significantly interacting with the ACE2 receptor, was the structure of daclatasvir, used in the treatment of HCV.

We initially asked ourselves if the results were incorrect. However, other researchers also used *in silico* approaches to the interaction of ivermectin with SARS-CoV-2 receptors, and found that the interaction was theoretically expressive (Eweas, Alhossary, & Abdel-Moneim, 2021; Guedes et al., 2021; Mody et al., 2021). The most recent research available from a randomized clinical trial with 476 patients found that the duration of symptoms of COVID-19 was not statistically significant among patients administered over 5 days with ivermectin compared to the placebo group. Thus, the results did not support the use of ivermectin for the treatment of COVID-19, although it highlighted the need for further studies with a larger sample of patients (López-Medina et al., 2021). Despite the theoretically promising results, to date there are no rigorous and peer-reviewed clinical studies proving its effectiveness. In the next section regarding the prediction of the degree of specificity of interaction, we were able to discover a possible theoretical cause of failures in clinical studies.

**Table 2.** Relative values of  $\Delta G^\circ$  ( $kcal \cdot mol^{-1}$ ) of interaction with some important receptors involved in the viral replication process and other signaling pathways.

Ligand	SARS-CoV-2 Mpro	RdRp Nsp12	SARS-CoV 3CLpro	TMPRSS2	SARS-CoV-2 S2	sIL-6R	PICALM	Sigma-1	Neurophilin-1	$\Delta G^\circ$
Ledipasvir	-9.4	-10.7	-11.6	-11.2	-10.7	-9.5	-9.0	-10.3	-11.3	-10.3
Dihydroergotamine	-9.9	-10.1	-11.8	-10.9	-10.2	-10.2	-9.2	-9.8	-9.8	-10.2
Paritaprevir	-9.5	-10.6	-12.1	-11.4	-10.4	-10.5	-8.6	-10.3	-10.0	-10.2
Ergotamine	-9.7	-10.1	-11.4	-10.9	-10.6	-9.0	-8.6	-10.1	-9.5	-9.9
Elbasvir	-8.7	-10.4	-11.2	-10.5	-11.0	-9.4	-8.9	-9.2	-10.2	-9.8
Ivermectin (b1b)	-8.4	-9.4	-11.0	-10.8	-11.2	-8.6	-7.7	-8.6	-9.7	-10.4
Ivermectin	-9.3	-10.2	-10.8	-10.3	-9.4	-10.6	-8.5	-9.3	-9.9	-9.6
Simeprevir	-8.6	-9.8	-11.2	-11.0	-9.7	-8.0	-8.9	-9.4	-9.9	-9.6
Telesartan	-8.7	-9.5	-10.0	-10.7	-10.1	-8.5	-9.0	-10.0	-9.0	-9.5
Imatinib	-8.6	-9.6	-10.3	-10.8	-9.7	-8.0	-8.7	-9.3	-9.5	-9.4
Moxidectin	-8.3	-10.0	-12.2	-10.0	-9.0	-10.0	-8.4	-9.2	-9.2	-9.4
Nafamostat	-7.5	-8.8	-9.9	-10.0	-9.4	-7.6	-8.5	-11.1	-9.2	-9.2
Ivermectin (b1a)	-8.5	-9.6	-10.0	-10.1	-11.0	-8.1	-7.8	-9.3	-9.4	-9.2
Hesperidin	-8.7	-10.4	-10.7	-10.2	-9.3	-8.2	-7.5	-8.6	-8.5	-9.2
Lurasidone	-8.3	-9.2	-10.3	-10.9	-9.0	-7.8	-8.1	-9.9	-8.9	-9.2
Dacatasvir	-8.5	-9.1	-9.7	-10.8	-10.0	-8.2	-8.1	-8.3	-9.8	-9.1
Setrobutavir	-8.1	-10.2	-10.2	-9.6	-9.8	-8.3	-8.2	-8.6	-9.4	-9.1
Danoprevir	-9.1	-8.7	-10.5	-10.1	-10.1	-8.1	-8.0	-9.0	-8.8	-9.1
Theaflavin	-8.1	-9.9	-11.1	-10.1	-9.3	-7.6	-8.1	-8.3	-9.4	-9.1
Montelukast	-8.4	-9.7	-9.9	-10.0	-8.9	-7.4	-9.3	-9.3	-9.3	-9.0
Posaconazole	-8.8	-9.2	-9.8	-10.2	-9.3	-8.1	-8.4	-8.7	-9.6	-9.0
Tamapicillin	-7.8	-8.5	-10.1	-8.9	-8.6	-7.9	-9.1	-11.8	-8.7	-9.0
Loprazolan	-7.9	-9.5	-10.5	-10.0	-8.6	-7.4	-8.8	-9.2	-9.2	-8.9
Lopinavir	-7.9	-8.4	-9.4	-9.7	-8.3	-7.2	-9.3	-9.1	-9.1	-8.8
Itracozazole	-8.4	-8.8	-10.2	-9.8	-9.2	-8.3	-7.7	-8.3	-9.6	-8.8
Apilmod	-8.2	-8.3	-9.4	-10.1	-8.7	-7.1	-8.4	-8.9	-8.3	-8.7
Debigatran	-7.2	-8.4	-9.4	-8.6	-8.2	-7.3	-7.3	-11.7	-8.9	-8.6
Fosaprepitant	-7.8	-9.0	-10.7	-9.0	-8.6	-7.5	-9.2	-8.9	-8.3	-8.6
Doxorubicin	-8.2	-8.5	-10.0	-10.1	-8.3	-7.0	-8.2	-8.7	-8.5	-8.6
Cobicistat	-8.0	-8.8	-9.7	-10.1	-8.3	-7.3	-8.2	-7.3	-8.5	-8.4
Losartan	-7.5	-8.4	-8.6	-9.8	-8.5	-6.9	-8.2	-8.4	-8.9	-8.4
Rubitecan	-7.4	-9.2	-8.4	-9.9	-7.5	-7.5	-8.2	-8.8	-8.9	-8.4
Baricitinib	-8.1	-8.3	-9.6	-9.0	-8.6	-7.7	-8.0	-8.0	-9.0	-8.4
Remdesivir	-8.8	-8.7	-9.1	-8.5	-8.0	-6.9	-7.9	-8.2	-7.8	-8.3
Vitamin D3	-6.9	-8.1	-7.7	-8.3	-7.8	-6.5	-8.4	-11.7	-8.5	-8.3
Lapatinib	-8.2	-8.6	-9.0	-8.4	-8.7	-7.2	-7.8	-8.4	-9.1	-8.3
Fexofenadine	-7.4	-9.0	-8.3	-9.1	-8.0	-8.0	-8.9	-8.8	-7.3	-8.2
Dexamethasone	-7.1	-8.3	-8.7	-8.7	-8.0	-7.5	-8.0	-9.8	-8.2	-8.2
Plerixafor	-7.0	-8.5	-8.9	-9.2	-8.4	-7.4	-7.5	-8.0	-8.3	-8.2
Teloprevir	-8.2	-8.2	-9.5	-9.3	-8.7	-6.9	-8.6	-7.2	-8.5	-8.2
Ceforanide	-7.9	-7.9	-8.7	-8.6	-8.6	-8.0	-8.0	-9.9	-7.3	-8.2
Darunavir	-7.8	-9.1	-7.8	-9.1	-7.8	-6.2	-8.5	-7.5	-8.2	-8.1
Ritonavir	-7.2	-8.6	-9.5	-9.3	-7.9	-6.8	-7.2	-7.2	-8.7	-8.1
Camostat mesylate	-6.9	-7.7	-8.3	-8.7	-8.2	-7.2	-7.0	-9.5	-8.2	-8.0
Acalabrutinib	-7.4	-8.5	-9.1	-9.0	-8.2	-7.4	-7.6	-8.3	-8.4	-8.0
Heparin Sodium	-7.6	-9.1	-9.5	-8.1	-8.2	-7.9	-7.4	-7.3	-7.9	-8.0
Ceftolozane	-8.0	-8.7	-8.8	-7.6	-8.4	-6.6	-7.4	-8.3	-7.0	-8.0
Fosamprenavir	-7.5	-7.5	-8.5	-8.4	-8.1	-7.1	-7.3	-7.9	-7.6	-7.9
Azithromycin	-7.1	-8.1	-9.4	-7.8	-7.7	-6.0	-8.0	-7.3	-7.5	-7.7
Fluoxetine	-6.9	-7.1	-7.2	-8.6	-7.5	-8.1	-7.2	-9.1	-8.0	-7.6
Cloperastine	-6.2	-7.0	-7.1	-8.7	-7.6	-6.1	-7.2	-8.6	-6.9	-7.3
Ebselen	-6.7	-8.1	-7.5	-8.1	-7.6	-6.0	-7.5	-9.0	-8.0	-7.5
Simvastatin	-6.6	-8.2	-7.6	-9.3	-7.4	-5.8	-7.4	-9.4	-6.9	-7.4
Ly mecyline	-7.1	-7.9	-8.1	-8.7	-7.5	-6.0	-6.4	-7.5	-6.9	-7.4
Atorvastatin	-7.1	-7.8	-8.7	-7.9	-8.0	-6.8	-6.6	-7.1	-7.4	-7.4
Nitazoxanide	-6.9	-7.6	-7.6	-7.6	-6.9	-6.1	-7.2	-8.6	-6.9	-7.3
Dextromethorphan	-7.1	-7.4	-7.4	-6.7	-6.7	-6.3	-7.1	-7.5	-6.9	-7.2
Galdesivir	-7.0	-6.6	-7.0	-7.5	-6.8	-6.3	-7.1	-7.5	-7.3	-7.1
Clemastine	-6.6	-6.7	-6.8	-8.0	-7.5	-5.3	-7.0	-7.7	-6.8	-7.1
Cinanserin	-6.6	-6.9	-7.3	-8.1	-6.8	-5.9	-6.9	-7.9	-7.2	-7.1
Hydroxychloroquine	-6.0	-6.4	-6.6	-8.1	-6.5	-5.3	-7.1	-8.3	-7.4	-6.9
Coleicine	-6.5	-7.0	-6.9	-8.6	-6.9	-6.4	-6.1	-7.4	-7.0	-6.8
Chloroquine	-6.0	-6.5	-6.5	-8.2	-6.4	-5.1	-7.4	-8.1	-6.0	-6.7
Tenofovir	-6.5	-6.4	-7.0	-7.0	-6.6	-6.0	-6.3	-7.5	-6.7	-6.4
Colfosceril palmitate	-5.5	-6.1	-6.9	-6.5	-6.2	-5.1	-6.4	-6.6	-7.0	-6.7
Ribavirin	-6.1	-6.4	-6.4	-7.1	-6.1	-5.6	-6.3	-6.0	-6.2	-6.4
Fingolimod	-5.2	-6.2	-6.0	-6.5	-6.6	-4.6	-6.9	-8.3	-6.6	-6.3
Umifenovir	-6.6	-7.3	-7.0	-7.0	-6.2	-5.3	-6.0	-6.5	-6.2	-6.3
Oseltamivir	-6.4	-6.1	-6.4	-7.1	-6.2	-5.3	-6.6	-6.8	-5.9	-6.2
Favipiravir	-5.7	-5.8	-5.9	-6.1	-5.7	-5.5	-5.9	-6.3	-6.3	-5.9
Captopril	-5.3	-5.4	-5.4	-5.7	-5.1	-4.4	-5.1	-5.9	-5.3	-5.3

#### 4.1.2. *The promising ledipasvir and others anti-HCV*

The two drugs administered to treat HCV (Hepatitis-C virus), ledipasvir and daclatasvir, were theoretically extremely promising with both viral receptors and the pro-inflammatory cytokine sIL-6R, with mean values of  $-10.2$  and  $-9.1 \text{ kcal} \cdot \text{mol}^{-1}$ , respectively. The ledipasvir complex with the sIL-6R protein resulted in remarkable interactions (see Figure 5), so that there were 3 carbonyl interactions, a total of 17 hydrogen bonds, 141 hydrophobic contacts, and the formation of 4 ionic interactions in addition to a total of 5 aromatic contacts in the complex. This therefore reflects directly on the interaction-free energy, which was remarkable in comparison to all the medications analyzed. Nevertheless, although the ledipasvir compound obtained by *in silico* approaches is theoretically effective in modulating SARS-CoV-2 receptors in addition to the pro-inflammatory pathway, preclinical and clinical studies would still be essential.

Paritaprevir showed significant binding affinity with SARS-CoV-2 Mpro and SARS-CoV-2 3CLpro, mainly due to the combination of two factors: a) the interaction via hydrogen bond with the Threonine residue (Thr199A and Thr169A); b) great hydrophobic interaction with the drug's alicyclic chain. Similar behavior is seen with the Nsp12 RNA polymerase receptor (see Figure 5). The results seem to suggest that the drugs with the highest affinity are those with significant hydrogen bonds and therefore with a large number of non-covalent interactions.

Unexpectedly even drugs structurally diverse and distinct in several aspects, the interaction with the respective binding site of each receptor proved to be remarkable, allowing us to conclude that potential repositioning drugs, *a priori*, do not necessarily have radicals or functional groups in common. Although docking simulations have their limitations, they are an essential approach when analyzing many ligands and receptors. Thus, based on the docking results, we could then prioritize certain drugs for further studies *in silico* or even experimental trials.

Dabigatran exhibited unexpected behavior with Sigma-1R, with an interaction-free energy of  $-11.5 \text{ kcal} \cdot \text{mol}^{-1}$ , possibly due to the large number of Hydrogen bonds from its carboxyl and amine groups. However, this behavior is not verified with the others receptors and proteases. The drug montelukast, administered to patients affected by

various asthma conditions, showed a significant interaction with sIL-6R, reinforcing that the mechanism in respiratory diseases may be to minimize the hyperinflammatory process. However, the interaction with viral receptors was a little less expressive. Based on the docking results, it appears that drugs for diseases apparently without any correlation with each other have similar  $\Delta G^\circ$  values and therefore have significant interactions with SARS-CoV-2 receptors. It is noteworthy that different drugs, with different functions, structures and purposes, have shown great affinity with the various biomolecules that could significantly affect the virus. However, many drugs also showed  $\Delta G^\circ$  values below the average of the best results obtained. Some pattern, whether structural or functional, is expected to become noticeable as more drugs are tested. The aminoquinolines chloroquine and hydroxychloroquine indicated low interaction affinity, either in viral or pro-inflammatory signaling, with  $\Delta G^\circ$  of  $-6.9kcal \cdot mol^{-1}$  and  $-6.7kcal \cdot mol^{-1}$ , respectively.

It is important to highlight the role of anticoagulants in the modulation of viral receptors, such as the nafamostat ligand, presenting significant interaction with Sigma-1 receptors with  $-11.1kcal \cdot mol^{-1}$ , and average value when analyzing all receptors  $-9.3kcal \cdot mol^{-1}$ , which can be an effective substitute for heparin or even administered as an adjuvant. In addition, the results corroborate the in vitro studies (Hoffmann et al., 2020) with regard to its ability to minimize the activation of the SARS-CoV-2 virus, in addition to having a greater potential for modulation in relation to mesylate of camostate.

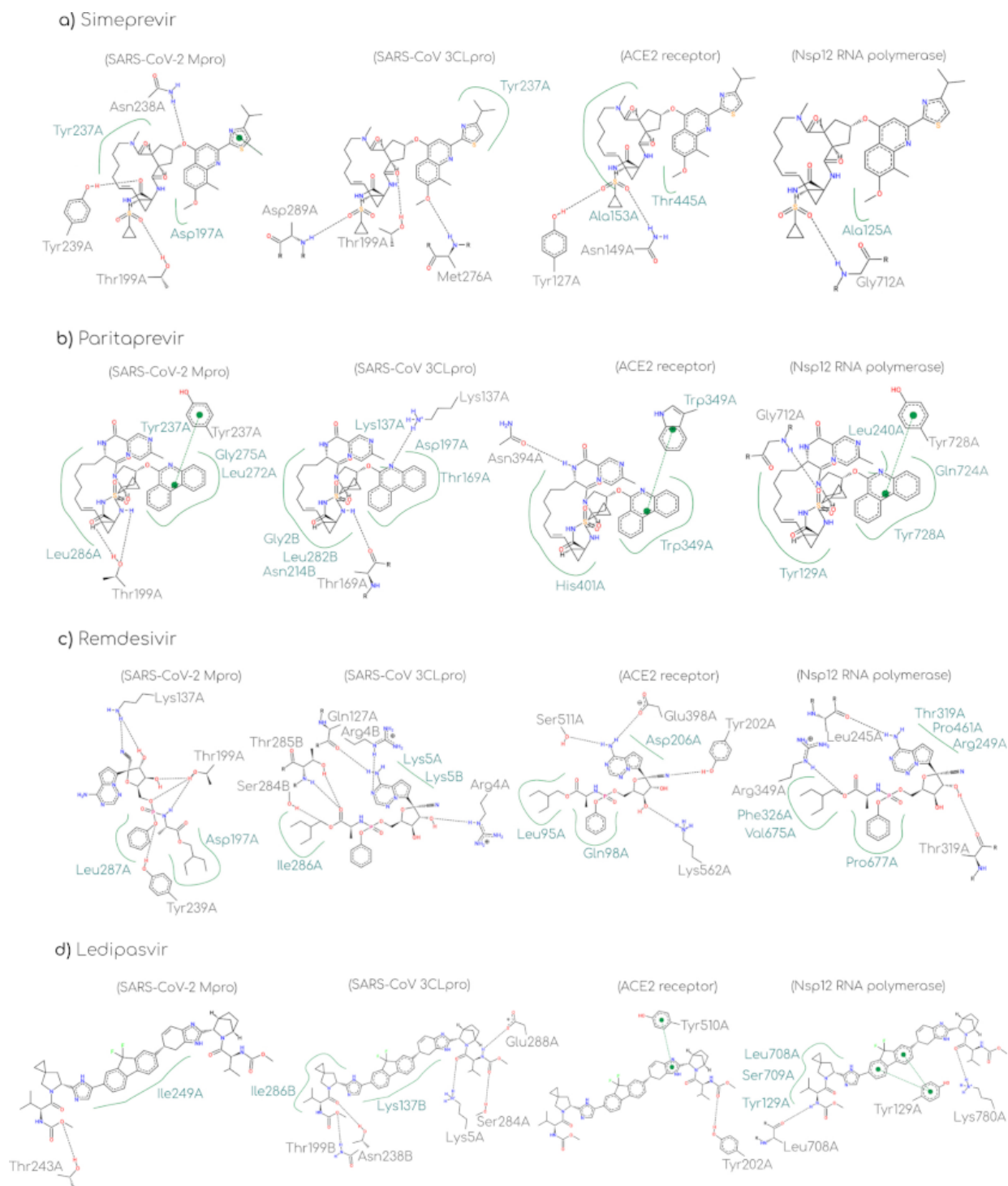


**Figure 5.** 2D diagrams of interaction of amino acids with the structure of ledipasvir and other theoretically promising medications. All diagrams were created using the ProteinPlus (Stierand & Rarey, 2010) tool. The dashed black lines represent non-covalent interactions (Hydrogen or metallic bonds). The green dashed lines correspond to hydrophobic contacts. Finally, the dashed green lines refer to interactions by stacking  $\pi - \pi$ .

#### 4.2. Prediction of interaction specificity

Finally, when analyzing the compounds with the highest average free energy score, we realized that some can be classified as “frequent hitters” or false positives, as they interact with several receptors (see Table 3) in addition to having a high probability of nonspecificity (see Table 4). According to the developers of the Hit Dexter 2.0 platform (Stork, Chen, Šícho, & Kirchmair, 2019), predictions via the degree of specificity via neural networks can help in the decision and priority of the experiments, but we cannot strictly consider the results. Due to the incidence of false positives, we propose to compare the 12 (twelve) compounds with the highest scores against a receptor not directly correlated to viral replication, the 5-*HT*<sub>1B</sub> serotonin reuptake receptor (PDB ID: 4IAQ) and the glutamate receptor GluR2 (PDB ID: 5H8S). From these results, it is perceived that it is totally contradictory that ivermectin could be administered to patients affected by depressive or generalized anxiety disorder only because the affinity with CNC recipients was expressive. That is why deeper *in silico* studies are extremely important, in addition to experimental tests to validate the conclusions.

Ledipasvir presented a specificity percentage probability of 79%, being therefore a much more selective medication than dihydroergotamine even with similar free energy values. Although ivermectin has shown promising results in docking, it was classified as a false positive due to the expressive nonspecificity of 93%. Therefore, the incidence of false positives is one of the most frequent limitations in docking simulations. Thus, in order to minimize flaws, the ideal would be validation through molecular dynamics or the future performance of enzymatic assays *in vitro* for different virus pathways, either for pro-inflammatory receptors or even at the CNC.

**Table 3.** Docking results for drugs of low specificity for receptors not directly correlated to viral replication.

Ligand	5-HT <sub>1B</sub>	Glutamate receptor (GluR2)	$\overline{\Delta G^\circ}$
Ledipasvir	-11.4	-11.5	-11.5
Dihydroergotamine	-10.8	-10.5	-10.6
Paritaprevir	-11.5	-12.2	-11.8
Ergotamine	-10.1	-10.3	-10.2
Elbasvir	-9.9	-9.2	-9.5
Ivermectin (b1b)	-9.3	-11.1	-10.2
Ivermectin	-9.5	-11.4	-10.4
Simeprevir	-11.7	-10.4	-11.0
Telmisartan	-12.2	-9.2	-10.7
Imatinib	-12.1	-9.8	-10.9
Moxidectin	-11.0	-9.7	-10.3
Nafamostat	-10.3	-8.5	-9.4
Ivermectin (b1a)	-9.8	-11.0	-10.4
Hesperidin	-10.4	-9.3	-9.8
Lurasidone	-11.4	-10.2	-9.1
Daclatasvir	-10.2	-9.4	-9.8
Setrobuvir	-10.7	-10.6	-9.6
Danoprevir	-8.6	-8.6	-8.9
Theaflavin	-10.9	-10.9	-9.6
Montelukast	-11.2	-8.3	-9.7
Posaconazole	-8.9	-9.4	-9.2
Talampicillin	-9.9	-9.9	-8.9

**Table 4.** Results of the prediction of the likelihood of a ligand being classified as “frequent hitter”. The two machine learning approaches available on the Hit Dexter 2.0 (Stork et al., 2019) platform were adopted, being trained with PSA (primary screening tests) and CDRA (confirmatory dose-response assays) in the predictive calculation for highly false positives. All predictions of physical-chemical parameters and violations of the Lipinski filter were made using the SwissADME (Daina, Michielin, & Zoete, 2017) platform. The values of  $pK_a$  under the alkaline condition were obtained from the DrugBank database by prediction in the MarvinSketch plugin.

Ligand	PSA	CDRA	Molar mass ( $g \cdot mol^{-1}$ )	$c \log P$	$pK_a$	RO5 violations
Ledipasvir	0.21	0.20	889.00	6.39	5.29	2
Dihydroergotamine	1.00	1.00	583.68	2.08	8.39	1
Paritaprevir	0.24	0.14	765.88	3.15	2.64	2
Ergotamine	0.91	0.72	581.66	2.27	7.78	1
Elbasvir	0.15	0.19	882.02	5.43	6.06	2
Ivermectin	0.93	0.38	1737.16	6.63	-3.4	3
Simeprevir	0.20	0.20	749.94	4.28	1.61	2
Telmisartan	0.15	0.14	514.62	5.98	6.13	2
Imatinib	0.21	1.00	493.60	3.38	8.27	0
Moxidectin	0.33	0.42	639.82	4.95	2.81	1
Nafamostat	0.27	0.46	347.37	2.11	11.32	0
Hesperidin	0.00	0.00	610.56	-1.06	-3.6	3
Lurasidone	0.24	0.22	492.68	4.13	8.5	0
Daclatasvir	0.13	0.16	738.87	4.14	6.09	2
Setrobuvir	0.17	0.14	560.62	2.22	0.69	1
Danoprevir	0.21	0.25	731.83	2.70	-3.5	2
Montelukast	1.00	1.00	586.18	7.20	3.12	2
Posaconazole	0.19	0.29	700.78	4.36	3.93	2
Talampicillin	0.18	0.13	481.52	2.04	7.23	0

## 5. Molecular dynamics for protein-ligand complex

The RMS analysis based on public data is found in (see Figure 6 and Table 5) where the complex of 8 (eight) drugs with the glycoprotein Spike was studied. The trajectories resulting from the MD are very sensitive to any numerical noise compared to other less complex computational methods. In this way, longer time intervals guarantee a greater probability of convergence and smaller disparities between two simulations carried out under the same conditions. Therefore, it was very important to complement the docking results with simulations of about  $2\mu s$ , enough to minimize biased conclusions.

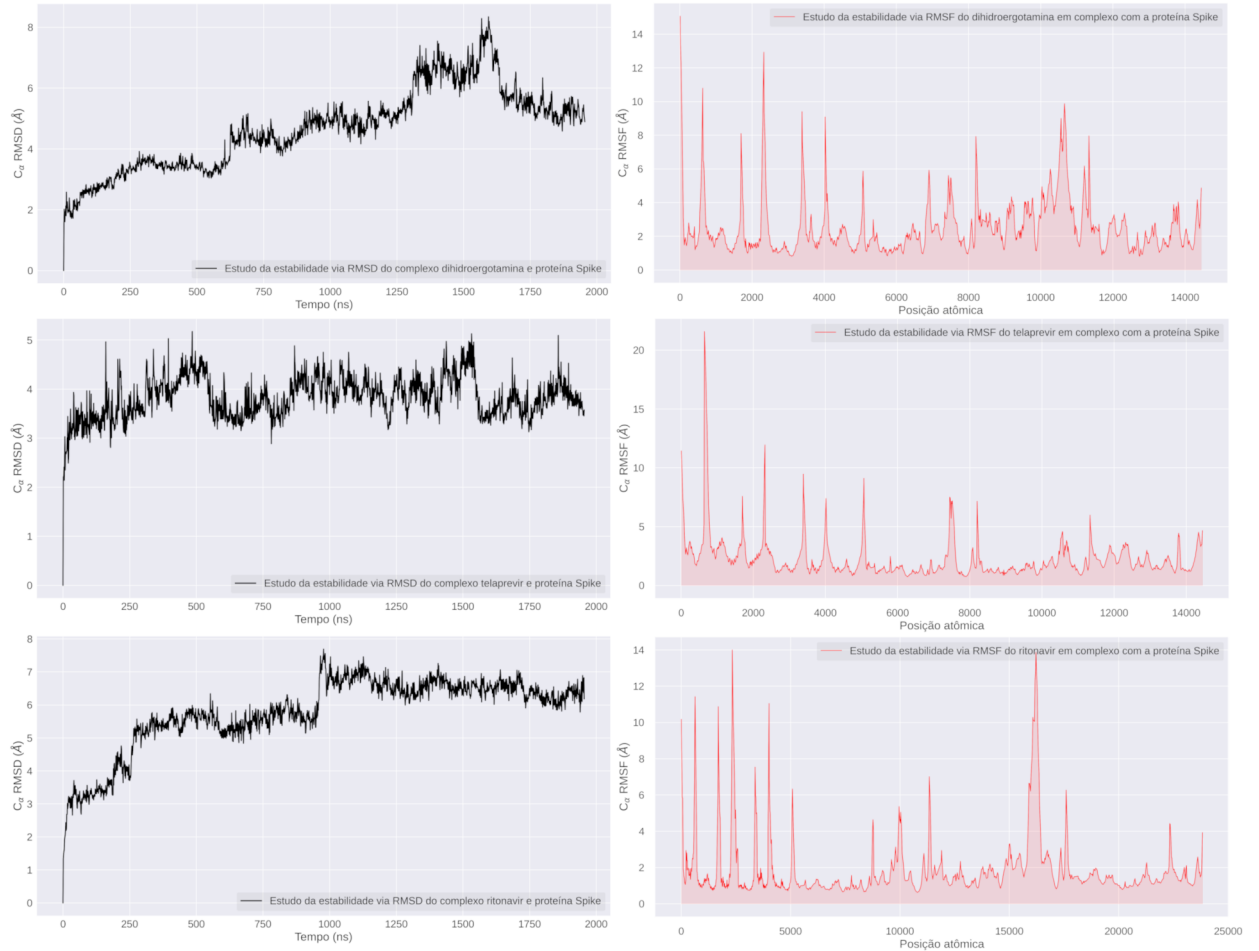


**Figure 6.** Simulations at about  $2\mu s$  with the drugs dihydroergotamine, telaprevir and ritonavir. The RMS analyzes are presented in relation to the  $C\alpha$  of the protein-ligand complex.

First of all, it should be noted that the structural flexibility in the receptor can contribute both to increase the affinity with the ligand and on the contrary. This will depend on whether the ligand molecules are highly rigid, where increased structural fluctuation will critically reduce affinity for the drug. In contrast, there will be an opposite behavior for more flexible molecules, where increased mobility in the receptor would make the binding affinity even greater (Forrey, Douglas, & Gilson, 2012). Consequently, greater fluctuations are an indication of more significant conformational changes and, therefore, when there are ligands with few degrees of rotational freedom, the  $\Delta G^\circ$  affinity tends to decrease. In general, we can summarize that the greater instability of the ACE2-RBD complex reflects greater difficulty for the cellular entry of the virus, and in this way we can measure the potential for modulation of a

medication.

The drug dihydroergotamine showed fluctuation peaks around 14Å, but due to the low flexibility of the medication, the affinity with Spike could be impaired. When the mean stability is analyzed, it is perceived to be the drug that caused the least mobility of all in Spike protein and, therefore, corroborating the docking results referring to the expressive modulatory activity against the virus. In other words, in this case the greater interaction affinity was reflected in greater Spike protein instabilities observed by molecular dynamics.

A notable conclusion is the potential for modulating the medicine telaprevir and due to its great flexibility, the significant peaks of atomic fluctuations in about 20Å express a remarkable interaction affinity with the Spike protein. As for the average values, it expressed the second highest average RMSD among those analyzed, which also corroborates the docking results. Similar results refer to ritonavir with fluctuation peaks of approximately 14Å, which expressed one of the highest RMSD averages among those analyzed. The high flexibility of ritonavir was in line with the significant instability in the protein Spike. On the other hand, the RMSF fluctuations were not significant and very similar to drugs with similar results in docking, such as telaprevir and darunavir.

Meanwhile, the antiparasitic nitazoxanide generated relatively high peak fluctuations around 10Å. Although the RMS average resembles more promising medications according to docking, for this case where the ligand is not very flexible, a high peak fluctuation is an important indication that the modulation of the viral receptor was not as expressive compared to the other medications.

The drug atorvastatin, as its affinity is more flexible, may have suffered a decrease due to lower fluctuation peaks of around 10Å. Thus, the non-significant result in docking and very similar to nitazoxanide was directly reflected in insignificant fluctuations in this medication. In turn, the drug captopril would be recommended for lower fluctuation peaks as it has only 3 rotatable bonds, but the mobility was relatively high with RMSF peaks close to 12Å, thus decreasing the affinity with the receptor. Although it presented one of the least promising results in docking, when the average fluctuations were analyzed, the difference was not as significant compared to other medications.

Consequently the explanation is the non-conformity between the low number of rotatable bonds while there were relatively high fluctuations in the Spike protein. The same observation applies to tenofovir with peak fluctuations of around 10Å. The higher average stability RMSD and RMSF among all is an indication of a reasonable interaction with the Spike protein as a result of the median ligand flexibility, where greater instability in the receptor is expected. In any case, the estimated affinity for docking expressed an average lower than several medications, and whose molecular dynamics partially reflected this result, probably due to the implicit consideration of water molecules. The darunavir drug, in turn, being highly flexible had a fluctuation peak close to 14Å, which is a promising result due to the high degree of rotational freedom. However, the mean RMSF value was among the lowest found, indicating that only very specific regions of the Spike protein underwent significant conformational changes.

In the context of Hydrogen bonds, there were no statistically significant differences between the medications analyzed. In spite of everything, it is important to note that the disregard for water molecules may have contributed to the Hydrogen bonds formed between the medications not showing notable differences between them.

**Table 5.** Average values of the RMSD and RMSF fluctuations of the complex between the simulated medications and the Spike protein in the closed conformation (PDB ID: 6VXX) in relation to Ca.

Ligand	Average RMSD	Average RMSF	Hydrogen bonds	Rotatable bonds
Nitazoxanide	$(3.532 \pm 0.407)\text{Å}$	$(2.112 \pm 1.244)\text{Å}$	$206 \pm 11$	4
Telaprevir	$(3.829 \pm 0.430)\text{Å}$	$(2.314 \pm 1.923)\text{Å}$	$207 \pm 12$	14
Dihydroergotamine	$(4.667 \pm 1.331)\text{Å}$	$(2.631 \pm 1.780)\text{Å}$	$205 \pm 12$	4
Atorvastatin	$(3.211 \pm 0.523)\text{Å}$	$(1.804 \pm 1.226)\text{Å}$	$210 \pm 12$	12
Captopril	$(3.480 \pm 0.595)\text{Å}$	$(1.767 \pm 1.408)\text{Å}$	$209 \pm 12$	3
Tenofovir	$(3.120 \pm 0.412)\text{Å}$	$(1.726 \pm 1.298)\text{Å}$	$205 \pm 12$	5
Darunavir	$(3.141 \pm 0.536)\text{Å}$	$(1.725 \pm 1.391)\text{Å}$	$213 \pm 12$	13
Ritonavir	$(5.770 \pm 1.096)\text{Å}$	$(2.045 \pm 1.998)\text{Å}$	$205 \pm 12$	18

Finally, we must note that the results of any computer simulation must always be seen with the perspective that the improvement of the force fields and algorithms is continuous and, therefore, these results are provisional until corroborated by more

in-depth theoretical studies or thorough experimental techniques.

## **6. Conclusions**

The results indicated that in terms of average free energy, ledipasvir, simeprevir and paritaprevir were among the main repositioning molecules. Although the structure of ivermectin has shown promising results, its probability of nonspecificity was practically total, leading to inconclusive answers about the pharmacological action. The drug nitazoxanide due to its low rotational freedom induced mean RMSD and RMSF fluctuations in the Spike protein above the normal, which, therefore, corroborates the few promising results obtained in molecular docking.

Despite the pro-inflammatory cytokine sIL-6R having a very consolidated role in the progression of COVID-19, as well as the receptors in the neurological system Sigma-1R and NRP-1, computational studies are still rare. In this way, we realized that most of the structures with remarkable interaction with viral receptors also formed a significant interaction with receptors in the neuroinflammatory system. Finally, we must emphasize that the safest way to eradicate outbreaks of coronavirus is with the administration of vaccines created specifically for this purpose. However, the results of this research are additions that may prove to be important in the context of an upcoming coronavirus pandemic, which may arise.

## **Conflicts of interests statement**

The authors declare no conflict of interest.

## **Funding information**

National Council for Scientific and Technological Development (CNPq) with grant 136222/2020 – 0.

## Acknowledgements

We express our gratitude to all researchers and people who came together to help each other in the fight against the SARS-CoV-2 virus. We are also grateful to the National Council for Scientific and Technological Development (CNPq) for supplying this project.

## Author contributions

*Kelson M. T. Oliveira*: led the project, writing-review and editing; *Micael D. L. Oliveira*: performed computational simulations, and takes responsibility for the integrity of the data as also accuracy of analyses.

## References

- Appleton, B. A., Wu, P., Maloney, J., Yin, J., Liang, W.-C., Stawicki, S., ... Wiesmann, C. (2007). Structural studies of neuropilin/antibody complexes provide insights into semaphorin and vegf binding. *The EMBO Journal*, *26*(23), 4902-4912.
- Bae, J. Y., & Park, H. H. (2011). Crystal structure of nalp3 protein pyrin domain (pyd) and its implications in inflammasome assembly. *Journal of Biological Chemistry*, *286*(45), 39528-39536.
- Berman, H. M., Westbrook, J., Feng, Z., Gilliland, G., Bhat, T. N., Weissig, H., et al. (2000). The Protein Data Bank. *Nucleic acids research*, *28*(1), 235-242.
- Bilinska, K., Jakubowska, P., Bartheld, C. S. V., & Butowt, R. (2020). Expression of the SARS-CoV-2 Entry Proteins, ACE2 and TMPRSS2, in Cells of the Olfactory Epithelium: Identification of Cell Types and Trends with Age. *ACS Chemical Neuroscience*. Retrieved from <https://doi.org/10.1021/acchemneuro.0c00210>
- Bolton, E. E., Chen, J., Kim, S., Han, L., He, S., Shi, W., et al. (2011). PubChem3D: a new resource for scientists. *Journal of cheminformatics*, *3*(1).
- Bursulaya, B. D., Totrov, M., Abagyan, R., & Brooks, C. L. (2003). Comparative study of several algorithms for flexible ligand docking. *Journal of Computer-Aided Molecular Design*, *17*(11), 755-763.
- Cantuti-Castelvetri, L., Ojha, R., Pedro, L. D., Djannatian, M., Franz, J., Kuivanen, S., ...

- Simons, M. (2020). Neuropilin-1 facilitates sars-cov-2 cell entry and infectivity. *Science*, *370*(6518), 856–860. Retrieved from <https://science.sciencemag.org/content/370/6518/856>
- Chen, Y., Liu, Q., & Guo, D. (2020). Emerging coronaviruses: Genome structure, replication, and pathogenesis. *Journal of Medical Virology*, *92*(4), 418-423.
- Daina, A., Michielin, O., & Zoete, V. (2017). SwissADME: a free web tool to evaluate pharmacokinetics, drug-likeness and medicinal chemistry friendliness of small molecules. *Scientific Reports*, *7*(1). Retrieved from <https://doi.org/10.1038/srep42717>
- Ellul, M. A., Benjamin, L., Singh, B., Lant, S., Michael, B. D., Easton, A., ... Solomon, T. (2020). Neurological associations of covid-19. *The Lancet Neurology*, *19*(9), 767 - 783.
- Eweas, A. F., Alhossary, A. A., & Abdel-Moneim, A. S. (2021). Molecular docking reveals ivermectin and remdesivir as potential repurposed drugs against sars-cov-2. *Frontiers in Microbiology*, *11*, 3602.
- Forli, S., Huey, R., Pique, M. E., Sanner, M. F., Goodsell, D. S., & Olson, A. J. (2016). Computational protein–ligand docking and virtual drug screening with the AutoDock suite. *Nature Protocols*, *11*, 905-919.
- Forrey, C., Douglas, J. F., & Gilson, M. K. (2012). The fundamental role of flexibility on the strength of molecular binding. *Soft Matter*, *8*, 6385-6392.
- Guedes, I. A., Costa, L. S. C., dos Santos, K. B., Karl, A. L. M., Rocha, G. K., Teixeira, I. M., ... Custódio, F. L. (2021, 03). Drug design and repurposing with DockThor-VS web server focusing on SARS-CoV-2 therapeutic targets and their non-synonym variants. *Scientific Reports*, *1*(1).
- Guilloux, V. L., Schmidtke, P., & Tuffery, P. (2009). Fpocket: An open source platform for ligand pocket detection. *BMC Bioinformatics*, *10*(1). Retrieved from <https://doi.org/10.1186/1471-2105-10-168>
- Hackos, D. H., Lupardus, P. J., Grand, T., Chen, Y., Wang, T.-M., Reynen, P., et al. (2016). Positive Allosteric Modulators of GluN2A-Containing NMDARs with Distinct Modes of Action and Impacts on Circuit Function. *Neuron*, *89*(5), 983-999.
- Heidary, F., & Gharebaghi, R. (2020). Ivermectin: a systematic review from antiviral effects to covid-19 complementary regimen. *The Journal of Antibiotics*, *73*(9), 593-602.
- Hoffmann, M., Kleine-Weber, H., Schroeder, S., Krüger, N., Herrler, T., Erichsen, S., et al. (2020). SARS-CoV-2 Cell Entry Depends on ACE2 and TMPRSS2 and Is Blocked by a Clinically Proven Protease Inhibitor. *Cell*, *181*(2), 271-280. Retrieved from <https://>

[doi.org/10.1016/j.cell.2020.02.052](https://doi.org/10.1016/j.cell.2020.02.052)

- Hu, J., Liu, Z., Yu, D.-J., & Zhang, Y. (2018). LS-align: an atom-level, flexible ligand structural alignment algorithm for high-throughput virtual screening. *Bioinformatics*, *34*(13), 2209-2218. Retrieved from <https://doi.org/10.1093/bioinformatics/bty081>
- Jubb, H. C., Higuero, A. P., Ochoa-Montaño, B., Pitt, W. R., Ascher, D. B., & Blundell, T. L. (2017). Arpeggio: A Web Server for Calculating and Visualising Interatomic Interactions in Protein Structures. *Journal of Molecular Biology*, *429*(3), 365-371. Retrieved from <https://doi.org/10.1016/j.jmb.2016.12.004>
- Leach, A. R. (2001). Molecular modelling principles and applications. In (2nd ed., p. 353). Pearson Education Limited.
- Liu, X., Zhang, B., Jin, Z., Yang, H., Rao, Z., et al. (2020). Structure of  $M^{pro}$  from COVID-19 virus and discovery of its inhibitors. *Nature*.
- Lovell, S. C., Davis, I. W., Arendall III, W. B., de Bakker, P. I. W., Word, J. M., Prisant, M. G., et al. (2003). Structure validation by  $\alpha$  geometry:  $\phi$ ,  $\psi$  and  $c\beta$  deviation. *Proteins: Structure, Function, and Bioinformatics*, *50*(3), 437-450. Retrieved from <https://doi.org/10.1002/prot.10286>
- López-Medina, E., López, P., Hurtado, I. C., Dávalos, D. M., Ramirez, O., Martínez, E., ... Caicedo, I. (2021, 03). Effect of Ivermectin on Time to Resolution of Symptoms Among Adults With Mild COVID-19: A Randomized Clinical Trial. *JAMA*.
- Mao, L., Jin, H., Wang, M., Hu, Y., Chen, S., He, Q., ... Hu, B. (2020, 06). Neurologic Manifestations of Hospitalized Patients With Coronavirus Disease 2019 in Wuhan, China. *JAMA Neurology*, *77*(6), 683-690.
- McCammon, J. A., Gelin, B. R., & Karplus, M. (1977). Dynamics of folded proteins. *Nature*, *267*(5612), 585-590.
- Michaud-Agrawal, N., Denning, E. J., Woolf, T. B., & Beckstein, O. (2011). MDAAnalysis: A toolkit for the analysis of molecular dynamics simulations. *Journal of Computational Chemistry*, *32*(10), 2319-2327.
- Miller, S. E., Sahlender, D. A., Graham, S. C., Robinson, M. S., & Peden, A. A. (2011). The molecular basis for the endocytosis of small r-snares by the clathrin adaptor calm. *Cell*, *147*(5), 1118-1131.
- Mody, V., Ho, J., Wills, S., Mawri, A., Lawson, L., Ebert, M. C. C. J. C., ... Taval, S. (2021, 01). Identification of 3-chymotrypsin like protease (3CLPro) inhibitors as potential anti-SARS-CoV-2 agents. *Communications Biology*, *4*(1).

- Osipiuk, J., Jedrzejczak, R., Tesar, C., Endres, M., Stols, L., Babnigg, G., . . . Joachimiak, K. (2020). The crystal structure of papain-like protease of SARS CoV-2. *Protein Data Bank*. Retrieved from <https://www.rcsb.org/structure/6W9C>
- Pagadala, N. S., Syed, K., & Tuszynski, J. (2017). Software for molecular docking: a review. *Biophysical Reviews*, *9*(2), 91-102.
- Patrick, G. L. (2013). An Introduction to Medicinal Chemistry. In (5th ed., p. 215-247). Oxford University Press.
- Perola, E., Walters, W. P., & Charifson, P. S. (2004). A detailed comparison of current docking and scoring methods on systems of pharmaceutical relevance. *Proteins: Structure, Function, and Bioinformatics*, *56*(2), 235-249.
- D. E. Shaw Research. (2020). *Molecular Dynamics Simulations Related to SARS-CoV-2*. Retrieved from [http://www.deshawresearch.com/resources\\_sarscov2.html](http://www.deshawresearch.com/resources_sarscov2.html) (Shaw Research Technical Data, accessed on 03 September)
- Sanner, M. (1999). Python: a programming language for software integration and development. *Journal of molecular graphics & modelling*, *17*(1), 57—61.
- Schmidt, H. R., Betz, R. M., Dror, R. O., & Kruse, A. C. (2018). Structural basis for  $\sigma 1$  receptor ligand recognition. *Nature Structural & Molecular Biology*, *25*(10), 981-987.
- Schmith, V. D., Zhou, J. J., & Lohmer, L. R. (2020). The Approved Dose of Ivermectin Alone is not the Ideal Dose for the Treatment of COVID-19. *Clinical Pharmacology & Therapeutics*. Retrieved from <https://doi.org/10.1002/cpt.1889>
- Serdyuk, I. N., Zaccai, N. R., & Zaccai, J. (2007). Methods in Molecular Biophysics: Structure, Dynamics, Function. In (p. 931-939). Cambridge University Press.
- Song, Y., DiMaio, F., Wang, R. Y.-R., Kim, D., Miles, C., Brunette, T., et al. (2013). High-resolution comparative modeling with rosetta. *Structure*, *21*(10), 1735-1742. Retrieved from <https://doi.org/10.1016/j.str.2013.08.005>
- Stierand, K., Maaß, P. C., & Rarey, M. (2006). Molecular complexes at a glance: automated generation of two-dimensional complex diagrams. *Bioinformatics*, *22*(14), 1710-1716.
- Stierand, K., & Rarey, M. (2010). Drawing the PDB: ProteinLigand Complexes in Two Dimensions. *ACS Medicinal Chemistry Letters*, *1*(9), 540-545.
- Stork, C., Chen, Y., Šícho, M., & Kirchmair, J. (2019). Hit Dexter 2.0: Machine-Learning Models for the Prediction of Frequent Hitters. *Journal of Chemical Information and Modeling*, *59*(3), 1030-1043.
- Trott, O., & Olson, A. J. (2010). AutoDock Vina: Improving the speed and accuracy of

- docking with a new scoring function, efficient optimization, and multithreading. *Journal of Computational Chemistry*, 31(2), 455-461.
- Varghese, J. N., Moritz, R. L., Lou, M.-Z., van Donkelaar, A., Ji, H., Ivancic, N., . . . Simpson, R. J. (2002). Structure of the extracellular domains of the human interleukin-6 receptor  $\alpha$ -chain. *Proceedings of the National Academy of Sciences*, 99(25), 15959-15964.
- Wang, C., Jiang, Y., Ma, J., Wu, H., Wacker, D., Katritch, V., . . . Xu, H. E. (2013). Structural basis for molecular recognition at serotonin receptors. *Science*, 340(6132), 610-614. Retrieved from <https://science.sciencemag.org/content/340/6132/610>
- Wang, W., Bodiga, S., Das, S. K., Lo, J., Patel, V., & Oudit, G. Y. (2012). Role of ace2 in diastolic and systolic heart failure. *Heart Failure Reviews*, 17(4), 683-691. Retrieved from <https://doi.org/10.1007/s10741-011-9259-x>
- Wang, X., Lan, J., Ge, J., Yu, J., Shan, S., et al. (2020). Structure of the SARS-CoV-2 spike receptor-binding domain bound to the ACE2 receptor. *Nature*, 581(7807), 215-220.
- Xia, S., Liu, M., Wang, C., Xu, W., Lan, Q., Feng, S., . . . Du, L. (2020). Inhibition of sars-cov-2 (previously 2019-ncov) infection by a highly potent pan-coronavirus fusion inhibitor targeting its spike protein that harbors a high capacity to mediate membrane fusion. *Cell Research*, 30(4), 343-355.
- Xu, X., Han, M., Li, T., Sun, W., Wang, D., Fu, B., . . . Wei, H. (2020). Effective treatment of severe COVID-19 patients with tocilizumab. *Proceedings of the National Academy of Sciences*, 117(20), 10970-10975. Retrieved from [10.1073/pnas.2005615117](https://doi.org/10.1073/pnas.2005615117)
- Zhou, P., Yang, X.-L., Wang, X.-G., Hu, B., Zhang, L., Zhang, W., et al. (2020). A pneumonia outbreak associated with a new coronavirus of probable bat origin. *Nature*, 579(7798), 507 - 513.
- Zhu, N., Zhang, D., Wang, W., Li, X., Yang, B., Song, J., et al. (2020). A Novel Coronavirus from Patients with Pneumonia in China, 2019. *New England Journal of Medicine*, 382(8), 727-733.
- Zubair, A. S., McAlpine, L. S., Gardin, T., Farhadian, S., Kuruvilla, D. E., & Spudich, S. (2020, 08). Neuropathogenesis and Neurologic Manifestations of the Coronaviruses in the Age of Coronavirus Disease 2019: A Review. *JAMA Neurology*, 77(8), 1018-1027. Retrieved from <https://doi.org/10.1001/jamaneuro.2020.2065>